

Viscoelasticity-based MR elastography of skeletal muscle

Dieter Klatt^{1,3}, Sebastian Papazoglou^{1,3}, Jürgen Braun² and Ingolf Sack^{1,4}

¹ Department of Radiology, Charité-Universitätsmedizin, Berlin, Germany

² Institute of Medical Informatics, Charité-Universitätsmedizin, Berlin, Germany

E-mail: ingolf.sack@charite.de

Received 31 March 2010, in final form 19 August 2010

Published 15 October 2010

Online at stacks.iop.org/PMB/55/6445

Abstract

An *in vivo* multifrequency magnetic resonance elastography (MRE) protocol was developed for studying the viscoelastic properties of human skeletal muscle in different states of contraction. Low-frequency shear vibrations in the range of 25–62.5 Hz were synchronously induced into the femoral muscles of seven volunteers and measured in a cross-sectional view by encoding the fast-transverse shear wave component parallel to the muscle fibers. The so-called springpot model was used for deriving two viscoelastic constants, μ and α , from the dispersion functions of the complex shear modulus in relaxed and in loaded muscle. Representing the shear elasticity parallel to the muscle fibers, μ increased in all volunteers upon contraction from 2.68 ± 0.23 kPa to 3.87 ± 0.50 kPa. Also α varied with load, indicating a change in the geometry of the mechanical network of muscle from relaxation ($\alpha = 0.253 \pm 0.009$) to contraction ($\alpha = 0.270 \pm 0.009$). These results provide a reference for a future assessment of muscular dysfunction using rheological parameters.

Introduction

Tissue mechanics is increasingly recognized as a novel source of contrast in medical imaging. This development has been driven by the well-known sensitivity of macroscopic mechanical parameters to micro-structural properties of biological tissues. Current techniques of elastography are based on medical ultrasound or magnetic resonance imaging combined with static tissue deformation, transient shear waves, or continuous time-harmonic wave stimulation. Magnetic resonance elastography (MRE) (Muthupillai *et al* 1995, Plewes *et al* 1995) is particularly suited for measuring the shear modulus in living muscle tissue: (i) MRE is based on shear waves capable of mechanically stimulating tissue deep inside the body; and (ii) MRE allows the observation of full-strain wave fields with equal sensitivity

³ Both authors contributed equally.

⁴ Author to whom any correspondence should be addressed.

in arbitrary spatial directions. In skeletal muscle, the components of anisotropic wave fields are governed by different shear moduli which are specific relative to the principal axes of the muscle (Gennisson *et al* 2003, Sack *et al* 2002, Papazoglou *et al* 2005, 2006, Sinkus *et al* 2005, Romano *et al* 2005). In elastographic studies of muscle, the capability of MRE to measure wave fields is particularly useful for selectively observing the shear modulus either parallel or perpendicular to the fibers. The parallel shear elasticity of skeletal muscle has been measured in healthy volunteers (Dresner *et al* 2001, Sack *et al* 2002, Heers *et al* 2003, Jenkyn *et al* 2003, Uffmann *et al* 2004, Bensamoun *et al* 2006) and in patients (Basford *et al* 2002, Brauck *et al* 2007, Bensamoun *et al* 2007, Ringleb *et al* 2007), while in a few studies the perpendicular component of the shear modulus was also deduced (Gennisson *et al* 2003, Papazoglou *et al* 2005, 2006, Sinkus *et al* 2005, Gennisson *et al* 2005). While all these approaches are based on the assumption of a purely elastic material, only limited data about the viscoelastic properties of *in vivo* skeletal muscle are available (Domire *et al* 2009, Hoyt *et al* 2008, Deffieux *et al* 2009, Gennisson *et al* 2010). The lack of data is related to the challenge of measuring direction-dependent quantities in an extended dynamic range. Assuming a transversely isotropic and incompressible medium, three constitutive parameters, i.e. two shear moduli and one ratio of Young's moduli (parallel and perpendicular to the fibers), describe the anisotropic elastic behavior of the material (Papazoglou *et al* 2006). Measurement of the viscoelastic properties of muscle additionally requires the application of multiple driver frequencies. The complexity of this multiple-parameter problem even increases when different contraction states of muscle are considered as necessary for monitoring muscular dysfunction by elastography (Basford *et al* 2002, Brauck *et al* 2007, Bensamoun *et al* 2007). Therefore, this paper proposes a simplified yet physically consistent approach to performing an analysis of rheological properties of *in vivo* muscle within clinically applicable measurement times. The new method is based on single-component wave encoding within the isotropic plane of muscle. Therefore, through-plane motions in a cross-sectional view relative to the muscle fibers are excited and measured, resulting in images of the so-called fast transverse (FT) wave mode. This mode is characterized by the polarization of the transverse waves parallel to fibers. The high shear modulus along the principal axis of elasticity causes an acceleration of the wave, as opposed to the slow transverse (ST) wave mode, with polarization perpendicular to the main axis of the muscle. A multifrequency stimulation of FT waves combined with broadband motion encoding gives access to the dynamics of the complex shear modulus (G^*) parallel to the muscle fibers. The dispersion of G^* can be analyzed using the springpot model, which has been shown by *in vivo* MRE of liver (Klatt *et al* 2008, Asbach *et al* 2010), breast (Sinkus *et al* 2007) and brain (Sack *et al* 2009, Wuerfel *et al* 2010) to provide two consistent and reproducible viscoelastic constants of biological tissue. The springpot-inherent powerlaw can be interpreted by means of hierarchically ordered mechanical networks, which fulfill the conditions of thermodynamic compatibility (Friedrich 1991) and causality (Schiessel *et al* 1995). The geometry and connectivity of these networks are associated with cellular organization and vascularization of *in vivo* tissue. In polymer physics, mechanical lattices assembled by viscous beads connected via springs are widely used for modeling the experimentally observed G^* dynamics. Those generalized Gaussian structures (GGS) provide insight into the relationship between the micro-structure and macroscopic mechanical response of a polymer sample (Jurjiu *et al* 2002, Blumen and Jurjiu 2002). However, this concept has not yet been translated to *in vivo* biological systems due to the lack of consistent shear modulus data representing different viscoelastic (and thus structural) states. In this study, the dispersion of G^* is altered by an active contraction of femoral muscle. The deduced viscoelastic constants are discussed in the light of structural changes in hierarchically ordered mechanical networks. The results may extend our understanding about the relationship between *in vivo* viscoelastic

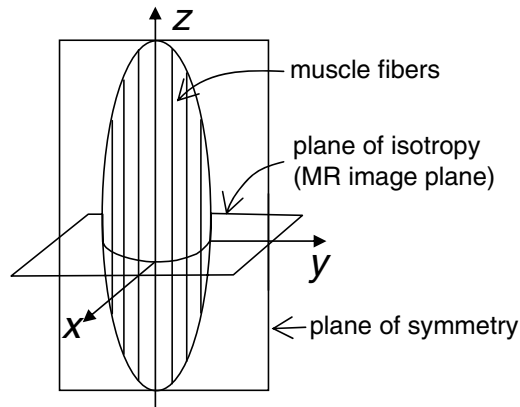


Figure 1. Coordinate system used in this study.

constants and physiological processes and may therewith help to interpret recent findings in MRE on patients (Sinkus *et al* 2007, Wuerfel *et al* 2010, Klatt *et al* 2008, Asbach *et al* 2008).

Theory

In this section, we briefly review the theoretical background of shear-wave-based elastography for the determination of muscle viscoelasticity, which requires the consideration of three major points:

- (i) anisotropic shear wave propagation in nearly incompressible media;
- (ii) dynamic modulus recovery by wave inversion;
- (iii) modeling of the dynamic behavior of the measured complex modulus.

Shear waves in incompressible, transversely isotropic media

In an anisotropic, linear elastic medium, three distinct modes of body waves exist for a given wave normal, $\mathbf{n} = [n_x, n_y, n_z]$ (Musgrave 1970). These modes are associated with three mutually orthogonal displacement vectors, \mathbf{u} , and are referred to as the longitudinal, the slow transverse (ST) and the fast transverse (FT) modes. The mode with the smallest angle between \mathbf{u} and \mathbf{n} is the longitudinal wave mode; however, its amplitude becomes infinitely small due to the assumption of incompressibility. Henceforth we will focus on the two remaining transverse modes and further employ a model of transversely isotropic elasticity with a constant alignment of the symmetry axis. This model exhibits the most basic representation of a material with a preferred direction of the elastic properties and is commonly used in elastography of skeletal muscle (Gennisson *et al* 2005, Papazoglou *et al* 2006). In our coordinate system, the axis of symmetry is z and the plane of isotropy is the x - y plane perpendicular to the muscle fibers (figure 1).

Using a plane wave solution for the equation of motion and solving the characteristic equation for the square of the phase velocity c^2 yield (Papazoglou *et al* 2006)

$$\begin{aligned} \rho c_{ST}^2 &= \mu_{xy}(n_x^2 + n_y^2) + \mu_{xz}n_z^2 \\ \rho c_{FT}^2 &= 4 \left(\mu_{xz} - \mu_{xy} \frac{E_z}{E_x} \right) \left(\frac{n_z^4}{\mathbf{n}^2} - n_z^2 \right) + \mu_{xz} \mathbf{n}^2, \end{aligned} \quad (1)$$

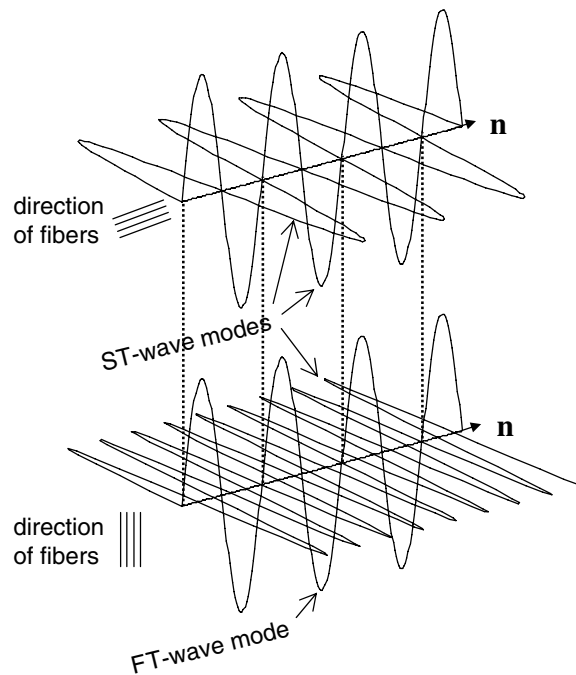


Figure 2. Sketch of shear oscillations corresponding to the slow transverse mode (ST) and the fast transverse mode (FT) defined by their polarization relative to the direction of muscle fibers ($\mu_{xz}/\mu_{xy} = 25/4$). Note that both ST- and FT-wave modes can exhibit equal wavelengths (indicated by dotted lines) and thus propagate with identical wave speeds.

with ρ being the mass density of the material. The ST mode is characterized by two distinct shear moduli, μ_{xy} and μ_{xz} , corresponding to shear deformations within the plane of isotropy and within the plane of symmetry, respectively. The FT mode additionally comprises a third parameter, the ratio of the axial elastic moduli (Young's moduli), E_z and E_x . According to equation (1), shear waves propagate with different speeds in anisotropic media corresponding to their polarization and direction. Figure 2 shows a sketch of two principal scenarios. In the upper graph, the shear wave propagates parallel to the muscle fibers so that all transverse polarizations are ST-wave modes. Since $\mathbf{n} = [0, 0, 1]$, we find a wavelength $\lambda_{ST} = \sqrt{\mu_{xz}/\rho}/f$ with f being the vibration frequency. Thus, although bearing the label 'slow', this mode is governed by the (usually) higher shear modulus μ_{xz} , rendering λ_{ST} large. In contrast, a wave propagating perpendicularly to the fibers ($n_x^2 + n_y^2 = 1; n_z = 0$) obeys both c_{FT} and c_{ST} , with $\lambda_{ST} = \sqrt{\mu_{xy}/\rho}/f$ and $\lambda_{FT} = \sqrt{\mu_{xz}/\rho}/f$. If the wave propagates in arbitrary directions, the *group velocity* has to be analyzed in order to deduce elastic constants from anisotropic wave patterns (Papazoglou *et al* 2006). The appearance of shear wave patterns in transversely anisotropic media is indicated in figure 3. MRE enables us to freely choose image plane position, encoding direction, i.e. the component of \mathbf{u} , and—depending on anatomy and actuator geometry—the direction of wave excitation. Thus, in a 2D image-based approach nine principal scenarios result, of which six are shown in figure 3. Here we propose a 2D quasi-isotropic scenario where—ideally—concentrically emanating wave fronts are measured without amplitude blanks related to the shear window, rendering the measured wave patterns suitable for modulus recovery by isotropic wave inversion. In muscle, this is only achievable by (1) choosing the image plane parallel to the plane of isotropy, (2) wave excitation

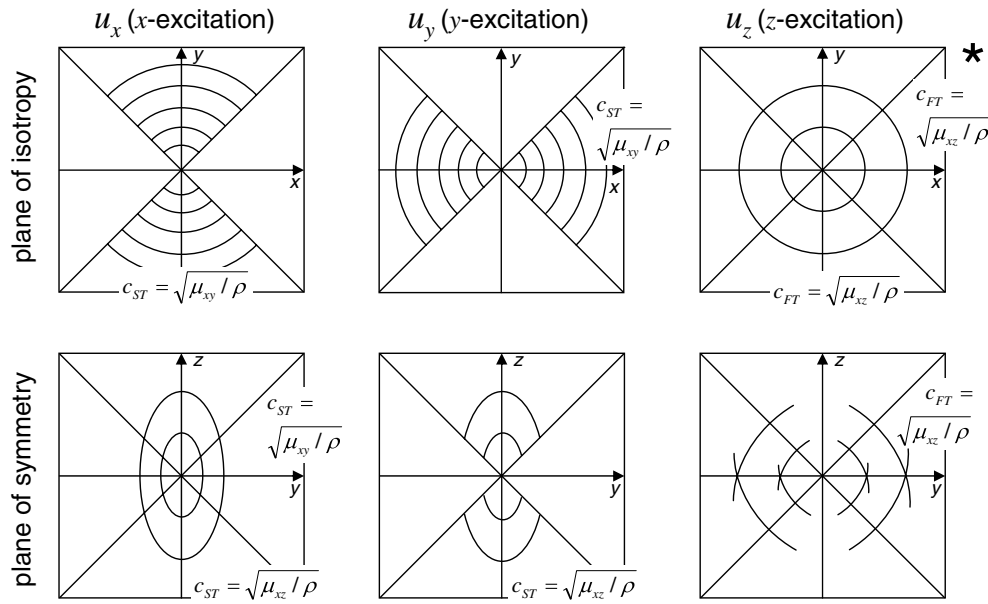


Figure 3. Two-dimensional schematic representations of shear-wave fronts of different polarizations in a transversely isotropic material ($\mu_{xz}/\mu_{xy} = 4$) emanating from a point source (which vibrates in the direction of wave polarization). The fibers are oriented parallel to the z -direction, as illustrated in figure 1. The wave velocities c_{ST} and c_{FT} according to equation (1) are indicated on the corresponding principal axes. The scenario that applies to the experiments is demarcated with an asterisk.

through-plane, i.e. parallel to the muscle fibers (in the z -direction) and (3) encoding this major motion component (u_z) by adjusting the motion-encoding gradient (MEG) along this direction. A sketch of this experimental scenario is given in figure 4. Obviously, a noninvasive approach requires an external wave stimulation that deviates from the internal focal stimulus given in figure 3. Instead, a vibrating ring was used for inducing inward propagating circular waves.

Complex shear modulus recovery

According to the correspondence principle (Carcione 2007), the solutions of the linear viscoelastic wave equation can be obtained from the solutions of the linear elastic wave equation in the frequency domain by replacing the components of the elasticity tensor, e.g. μ_{xz} , with the corresponding complex moduli, e.g. $G_{xz}^*(\omega)$. Therefore, our considerations of shear waves in an anisotropic elastic medium also hold for the viscoelastic case. Henceforth, $G_{xz}^*(\omega)$ is denoted as $G^*(\omega)$, which can be recovered from the aforementioned quasi-isotropic scenario by Helmholtz inversion (Klatt *et al* 2007):

$$G^*(\omega) = -\rho\omega^2 \frac{U(x, y, \omega)}{\Delta U(x, y, \omega)}, \quad (2)$$

where Δ denotes the Laplacian and $U(x, y, \omega)$ is the Fourier transform of $u_z(x, y, t)$, relating $G^*(\omega)$ to the symmetry plane of the muscle. In homogeneous media, $G^*(\omega)$ is not a function of space.

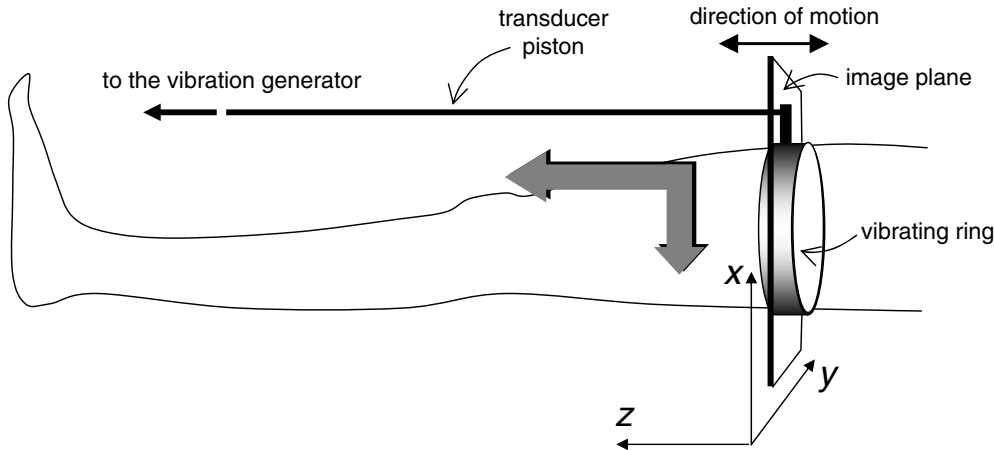


Figure 4. Experimental setup used for inducing FT shear waves into human thigh muscle. The gray arrows indicate the voluntary forces inside the leg imposed for isometric contraction of the M. quadriceps femoris.

Modeling the dynamics of the complex shear modulus

Skeletal muscle tissue is composed of many muscle fibers that consist of hundreds of myofibrils inside a matrix of cellular organelles (Schmalbruch 1985). According to the sliding filament model, muscle activation is due to the cross-linking of myofibril substructures, the myosin and actin filaments, which also exhibit a fiber-like geometry. The fiber architecture of muscle tissue at multiple hierarchic levels motivates the use of self-similar networks for modeling the rheological behavior of muscle tissue. $G^*(\omega)$ reflects the dynamic properties of such a viscoelastic network and is thus sensitive to the micro-structural constitution of the tissue under investigation. Depicting the viscoelastic network through beads subject to friction (with a friction coefficient ξ) and connected to each other by springs (with a spring constant K) leads to the Rouse model for chains (Rouse 1953) or to GGS for arbitrary mesh-like structures (Gurtovenko and Blumen 2005). The shear dynamics of a GGS is governed by the characteristic relaxation time $\tau_0 = \xi/K$ which, in the framework of classic viscoelastic models, is equivalent to $\tau = \eta/\mu$ with η and $\mu \equiv \mu_{xz}$ being the shear viscosity and shear modulus of a continuous sample, respectively. Single vibration modes of the network relax by characteristic times $\tau_k = \tau_0/\lambda_k$, which are determined by the eigenvalues λ_k of the connectivity matrix of the GGS. The superposition of all modes yields

$$G^*(\omega) = C \frac{1}{N} \sum_{k=2}^N \frac{i\omega\tau_k/2}{1 + i\omega\tau_k/2}, \quad (3)$$

where N is the number of viscous beads. C is related to the thermodynamic equilibrium of the GGS (see the appendix for further details). The first eigenvalue λ_1 corresponds to rigid translation of the whole GGS and is thus omitted from summation in equation (3). It is a general property of the GGS that the underlying structure is revealed in an intermediate dynamic range which shows scaling, i.e. powerlaw behavior ($G^* \sim \omega^\alpha$). For large N ($>10^3$ beads in a linear chain), this intermediate scaling behavior ranges from steady flow ($\omega = 0$) to a crossover frequency at approximately $\omega\tau_0 = 1$, where the material properties turn to solid-like, glassy behavior. In our experiments, the relaxation time τ is approximately

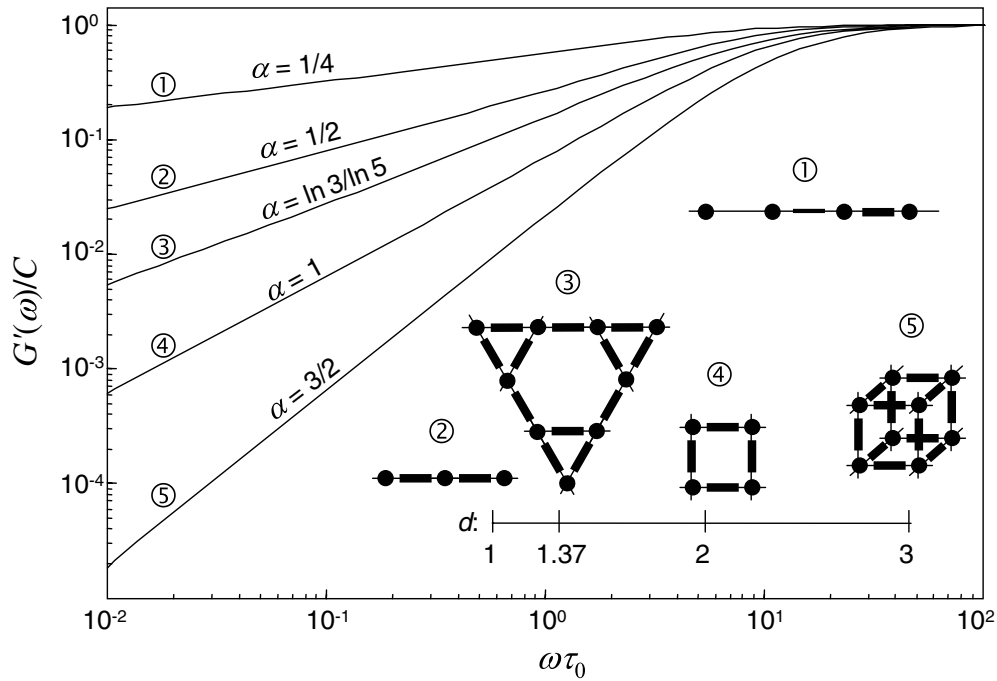


Figure 5. Fundamental characteristics of the scaling behavior of the reduced storage modulus in different structures. Numbers refer to fractal ladder hierarchy with changing spring constants (①), 1D Rouse chain (②), dual Sierpinski gasket (③), 2D regular lattice (④) and 3D cubic network (⑤). Corresponding structure elements are illustrated by bars for springs and dots for viscous beads (the fractal Sierpinski gasket is drawn without higher recursion levels). α -values indicate the slope of the $G'(\omega)$ function in the intermediate dynamic range, which is determined from half the dimension d of the structure. For ③ the spectral dimension of the fractal network was used given by $2\ln(d+1)/\ln(d+3)$ for a Sierpinski-type triangle with three connections embedded in the 2D Euclidian space (Blumen and Jurjiu 2002, Jurjiu *et al* 2002). Simulations were performed by numerical computations of eigenvalues λ_k of the connectivity matrix (A_{lm}) (see the appendix and equation (3)) with 10^5 (① and ②), 3^8 (③), $10^3 \times 10^3$ (④) and $10^2 \times 10^2 \times 10^2$ (⑤) beads. In ①, the strength of the spring constant at each mode k was increased with $K = \xi/\tau_0(k/N)^{2.5}$ (see the text for further details).

1.1 ms (taking values for storage and loss moduli measured later in this study), which yields a range of $\omega\tau$ between 0.17 and 0.45 for driving frequencies from 25 to 62.5 Hz. Thus, elastography can measure the powerlaw behavior of $G^*(\omega)$ as is numerically exemplified in figure 5 for the storage modulus $G' = Re(G^*)$ of some regular structures given by a Rouse chain, 2D, and cubic networks, as well as a fractal network based on a dual Sierpinski gasket. In the logarithmic plot, the structure-relevant intermediate range of G^* is displayed with the linear slope of $\alpha = d/2$, i.e. α equals half of the Euclidian dimension d . A more general relationship between α and the structure is obtained by employing the generalization of the integer-valued Euclidian dimension of regular lattices to the non-integer spectral dimension of fractal structures (Blumen and Jurjiu 2002). Generally speaking, α in the intermediate frequency range is determined by the degrees of freedom in the underlying GGS (and *not* by the details of the particular network structure), with values between $\alpha = 1/2$ for chains and $\alpha = 3/2$ for cubic networks. It was shown by Schiessel and Blumen (1995) that α can also take values below $1/2$ when representing the linear Rouse chain as a fractal ladder with increasing spring constants at each recursion level of self-similar expansion. As a result, the underlying

structure is no longer self-similar but hierarchical. A powerlaw with $\alpha < 1/2$, as has been determined in recent studies on biological tissue (Sack *et al* 2009, Wuerfel *et al* 2010, Asbach *et al* 2010), can be modeled through imposing a hierarchy on τ such that spring constants (or shear elasticity values) increase at each vibration mode k . Henceforth, we will adopt this mechanical realization of a powerlaw $G^* \sim \omega^\alpha$ with $0 < \alpha < 1$ using the springpot model (Klatt *et al* 2010):

$$G_S^* = \kappa (i\omega)^\alpha \quad \text{with} \quad \kappa = \mu^{1-\alpha} \eta^\alpha. \quad (4)$$

Since the shear modulus, μ , and the viscosity, η , are not independent in this model, we use a viscosity value $\eta = 1$ Pa s, yielding $\kappa = \mu^{1-\alpha}$. Different values of shear viscosity were assumed in studies on brain (Sack *et al* 2009, Wuerfel *et al* 2010) and liver (Asbach *et al* 2010); however, in the absence of experimental data we propose unity for viscosity, which simplifies equation (4) to $G_S^* = \mu^{1-\alpha} (i\omega)^\alpha$. Thus, κ is transformed to a variable of dimension of a shear modulus in accordance with the classical terminology of elastography. This transformation impacts neither the fit of $G^*(\omega)$ nor its phenomenological interpretation.

It is an inherent characteristic of the springpot model that storage and loss moduli, $G_S'(\omega)$ and $G_S''(\omega)$, display parallel lines in the logarithmic plot, i.e. α represents the slopes of *both* storage and loss moduli. Thus, the ratio of the real part and imaginary part of $G_S^*(\omega)$ is a constant given by

$$\alpha = \frac{2}{\pi} \arctan \left(\frac{G_S''(\omega)}{G_S'(\omega)} \right). \quad (5)$$

Materials and methods

Multifrequency MRE of M. quadriceps femoris dexter was performed in seven healthy male volunteers (mean age: 36.6 ± 6.5 years). Written informed consent was obtained from each subject. After examination of relaxed thigh muscle, the volunteers were asked to actively induce a maximum thigh muscle contraction by stretching the leg in plantar flexion with moderate voluntary pressure to the table. The induced contraction was approximately isometric due to the constant flexion angle of the leg and the foot (figure 4). Shear waves were introduced into thigh muscle by a ring-shaped actuator mounted via an extended piston to the vibration source. The source was based on a loudspeaker as described in Klatt *et al* (2006). The main vibration direction was in the head-foot direction perpendicular to the image plane. A sketch of the setup is shown in figure 4. For wave stimulation, a burst of 400 ms of a superposition of four harmonic vibrations was fed into the actuator. Vibration frequencies were 25, 37.5, 50 and 62.5 Hz with an increase in the harmonic amplitudes of 1, 4, 8 and 16 relative to the 25 Hz vibration, respectively. Measurements were performed on a 1.5T Siemens Sonata scanner using a single-shot spin-echo EPI (echo planar imaging) sequence sensitized to motion by a single cycle sinusoidal MEG of 20 ms duration, an amplitude of 35 mT m^{-1} , and direction perpendicular to the axial image plane. Further acquisition parameters were as follows: $165 \times 165 \text{ mm}^2$ field of view, 128×128 matrix size, 64 phase-encoding steps, 10 mm slice thickness, 1.56 kHz pixel bandwidth, 90° flip angle, 64 ms echo time, 1.5 s repetition time, 20 dynamics of the wave cycle with a 4 ms increment, interleaved MEG flips for calculating phase-difference images, and 60 s total scan time for one dynamic MRE scan.

The wave images were temporally Fourier-transformed yielding $U(x, y, \omega)$ for calculating $G^*(x, y, \omega)$ via equation (2) (with $\rho = 1050 \text{ kg m}^{-3}$). Before inversion, $U(x, y, \omega)$ was spatially filtered as described in Klatt *et al* (2007) for liver tissue. The complex shear modulus $G^*(x, y, \omega)$ was spatially averaged within a region of interest (ROI) given by the boundaries

Table 1. Averaged storage modulus (G'), loss modulus (G'') and modulus ratio of human femoral muscle at four drive frequencies (interindividual mean \pm standard deviation).

Vibration frequency	Relaxation			Contraction		
	G' (kPa)	G'' (kPa)	G''/G'	G' (kPa)	G'' (kPa)	G''/G'
25.0 Hz	0.77 \pm 0.14	0.31 \pm 0.09	0.40 \pm 0.06	0.67 \pm 0.07	0.27 \pm 0.04	0.40 \pm 0.03
37.5 Hz	1.18 \pm 0.15	0.47 \pm 0.07	0.40 \pm 0.03	1.41 \pm 0.16	0.50 \pm 0.10	0.36 \pm 0.04
50.0 Hz	1.52 \pm 0.10	0.54 \pm 0.06	0.35 \pm 0.03	2.05 \pm 0.19	0.80 \pm 0.06	0.39 \pm 0.03
62.5 Hz	2.02 \pm 0.14	0.69 \pm 0.08	0.34 \pm 0.02	2.67 \pm 0.27	0.96 \pm 0.14	0.36 \pm 0.02

of the M. quadriceps femoris visible in the MRE magnitude image. μ and α were determined by fitting equation (4) (with $\eta = 1$ Pa s) to the experimental modulus dispersion $G^*(\omega)$ using a least-squares routine. In this routine $\chi^2(\alpha, \mu)$ was calculated from $G^*(\omega)$ and $G_S^*(\omega)$ for α ranging from 0 to 1 in steps of 0.005 and for μ ranging from 0 to 50 kPa in steps of 0.25 kPa. The α and μ values corresponding to $\min(\chi^2)$ were used as new center values of smaller parameter ranges with higher resolution. The iteration was repeated until $\min(\chi^2)$ did not vary more than 100 Pa². Finally, the determined μ and α were averaged over three examinations in each volunteer and the corresponding intraindividual standard deviations (SD) were derived.

Results

Figure 6 shows shear waves in the quadriceps femoris muscle overlaid with standard T2-weighted magnitude images acquired in a volunteer. The real part of $U(x, y, \omega)$ in the relaxed muscle is illustrated in the upper row, while waves in the contracted muscle are presented at the bottom. An increase of wavelengths from top to bottom is perceptible, in particular, for $f = 50$ and 62.5 Hz. Further visual assessment is hampered by reverberations and large wavelengths in particular at lower drive frequencies. Wave inversion by equation (2) yielded four storage moduli (G') and four loss moduli (G''), whose values averaged over all individuals are listed in table 1. It can be clearly seen that muscle contraction is associated with an increase of the slopes of G' and G'' . Thereby, the ratios G''/G' remain widely constant within the given tolerance margins, indicating the validity of the powerlaw inherent to equations (4) and (5). Modeling by the springpot supports this result. The springpot variables α and μ in resting and in contracted femoral muscle (figure 7) are highly correlated upon contraction, i.e. the increase of μ is associated with an increasing parameter α . Despite considerable interindividual variances in both μ and α , the parameter ratios $\mu(\text{contracted})/\mu(\text{relaxed})$ and $\alpha(\text{contracted})/\alpha(\text{relaxed})$ in each volunteer exceed 1. In relaxed muscle, the smallest individual μ of all volunteers was 2.46 ± 0.32 kPa (volunteer 1), while the largest value was 3.09 ± 0.01 kPa (volunteer 2, see table 2), which displays a significant ($P < 0.05$) interindividual variation of relaxed muscle stiffness. Also in the contracted state, the difference between least volunteer muscle stiffness ($\mu = 3.31 \pm 0.30$ kPa, volunteer 3) and its maximum value ($\mu = 4.57 \pm 0.28$ kPa, volunteer 2) was significant. The ranges of $\mu(\text{relaxed})$ and $\mu(\text{contracted})$ do not overlap, in contrast to the large variability of α with overlapping ranges of $\alpha(\text{relaxed})$ and $\alpha(\text{contracted})$. The range of α in the relaxed state was between 0.241 ± 0.005 and 0.267 ± 0.001 , while the range in the contracted state was between 0.257 ± 0.008 and 0.287 ± 0.007 , resulting in significant interindividual variability ($P < 0.05$). It is important to mention that the evaluated regions

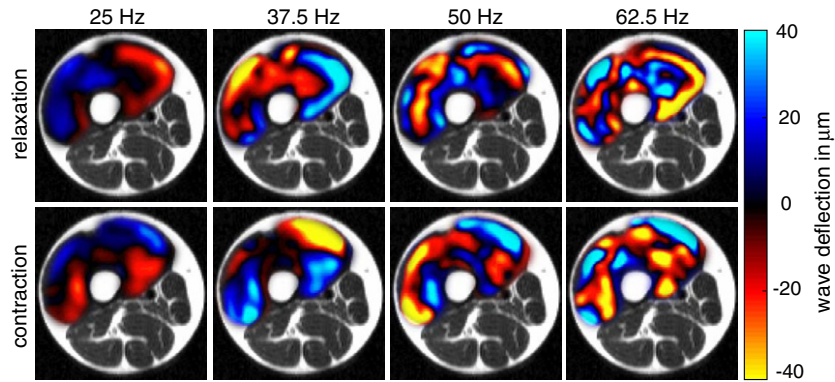


Figure 6. Experimental MRE waves $Re(U[x, y, \omega])$ (color coded) superimposed on T2-weighted MRI (field of view: 150 mm \times 150 mm) in a transversal image plane of the thigh of a volunteer. Top and bottom rows display experiments in relaxation and with maximum voluntary contraction, respectively.

Table 2. Individual viscoelastic parameters α and μ of the femoral muscle in relaxation and in contraction. Errors correspond to the standard deviation of three independent experiments; symbols refer to the graph in figure 7.

Volunteer	Symbol	Relaxation		Contraction	
		α	μ (kPa)	α	μ (kPa)
1	○	0.252 ± 0.007	2.46 ± 0.32	0.268 ± 0.009	3.33 ± 0.39
2	□	0.267 ± 0.001	3.09 ± 0.01	0.287 ± 0.007	4.57 ± 0.28
3	☆	0.241 ± 0.005	2.55 ± 0.10	0.257 ± 0.008	3.31 ± 0.30
4	▽	0.255 ± 0.023	2.74 ± 0.10	0.269 ± 0.021	3.92 ± 0.63
5	△	0.259 ± 0.002	2.53 ± 0.06	0.275 ± 0.015	4.47 ± 0.32
6	◁	0.243 ± 0.010	2.84 ± 0.03	0.268 ± 0.010	3.68 ± 0.19
7	▷	0.255 ± 0.004	2.52 ± 0.08	0.269 ± 0.003	3.81 ± 0.13
Mean		0.253 ± 0.009	2.68 ± 0.23	0.270 ± 0.009	3.87 ± 0.50

of M. quadriceps femoris were not significantly altered with interindividual mean values of $51.6 \pm 5.3 \text{ cm}^2$ in relaxation and $52.4 \pm 5.4 \text{ cm}^2$ in contraction. This is a strong indication that the deduced rheological constants are not biased by effects related to a change in macroscopic muscle geometry. Tables 1 and 2 summarize the mean moduli G' and G'' and the individual values of μ and α according to equation (4).

Discussion

Shear-wave-based elastography of muscle combines multiple effects arising from the specific functional and constitutive properties of skeletal muscle. In this study, the anisotropy of thigh muscle was addressed by exciting and encoding a specific FT-wave component; the dispersion of the complex modulus was measured at four distinct driving frequencies, and muscle function was initiated by alternating states of relaxation and contraction. Data analysis was based on two independent parameters μ and α of the springpot model both of which were

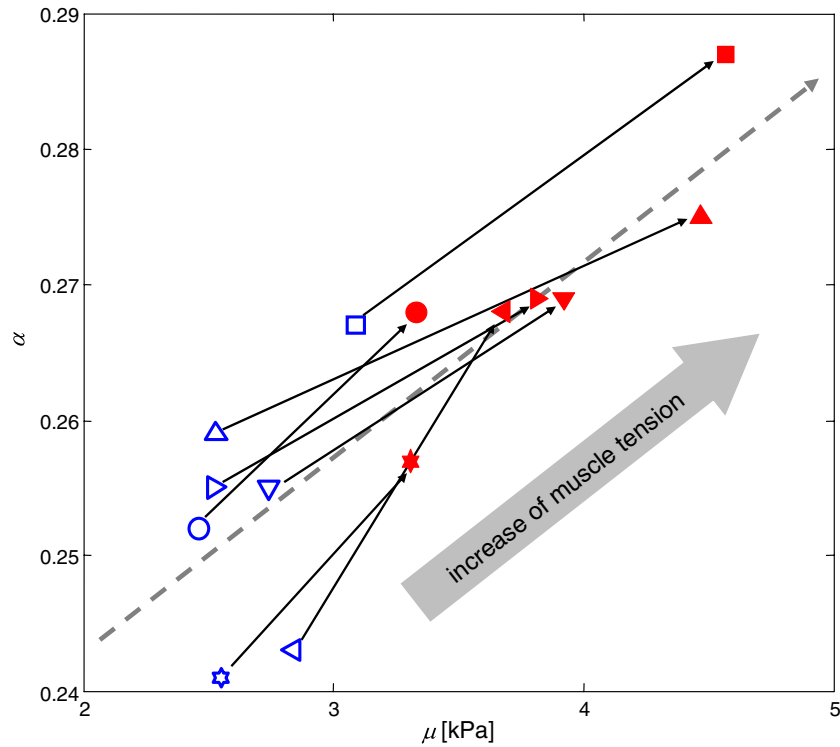


Figure 7. Individual viscoelastic constants according to the springpot model of the quadriceps femoris muscle in relaxation (blue, empty) and in contraction (red, filled). Each symbol refers to one volunteer as listed in table 2. The dashed line with a slope of $1.4 \times 10^{-5} \text{ Pa}^{-1}$ represents the mean of the data in both muscle conditions.

observed to increase with muscle contraction in all volunteers. It is important to mention that this observation does not depend on our assumption of a specific viscosity value η of muscle tissue. According to equations (4) and (5), α does not change with η while μ depends on η . However, the significance of μ is not affected by a changing η -parameter since its variability also changes. For example, assuming a viscosity $\eta = 10 \text{ Pa s}$, the shear modulus averaged over all volunteers clearly increases from $\mu = 1.23 \pm 0.10 \text{ kPa}$ in relaxation to $\mu = 1.64 \pm 0.15 \text{ kPa}$ in contraction.

A preliminary interpretation of this principal finding, i.e. the simultaneous increase of μ and α in activated muscle, can be based on simulations shown in figure 5 implying the following two points:

- (i) Supposing that the underlying structure is self-similar, we would expect an increase in the dimension of the fractal network upon contraction, as may result from the establishment of additional cross-links that change the degree of freedom in the entire network.
- (ii) The fact that we have observed $\alpha < \frac{1}{2}$ suggests a hierarchical order of spring constants with increasing rigidity toward smaller structures (e.g. myofibrils, fibers, sarcolemma, endomysium). An increase in α upon muscle contraction might then be caused by the increasing relevance of higher-ranking structures, as given by fiber bundles, fasciculus, or epimysium.

On the one hand, the establishment of cross-bridges between filaments changes the inherent geometry of muscle at a micro-structural level. On the other hand, structure-building elements in muscle from filaments to fiber bundles display a wide variety of mechanical properties which differ not only due to their intrinsic constituents but also by the variety of enwrapping (connective) tissues displaying different mechanical properties at different pre-stretch levels. We can therefore speculate about the superposition of changes in both geometry and hierarchy that takes place while the muscle is activated. Attempting to address the complex interplay between macro- and micro-mechanical constituents in muscle by scaling, one may regard cross-bridges between myosin and actin filaments as additional spring elements that are established by activation (Blange *et al* 1997) and thus change the degree of freedom in the mechanical network of muscle. It was therefore stimulating to observe, in analogy to this microscopic picture, an increasing slope α in our macroscopic G^* values upon contraction. In contrast, MRE studies of hepatic fibrosis showed no change in α with the degree of fibrosis (Klatt *et al* 2008, Asbach *et al* 2010). Also, MRE of brain revealed no change in α , neither in the course of physiological aging (Sack *et al* 2009) nor due to multiple sclerosis (MS) (Wuerfel *et al* 2010). In the context of the present results on muscle, it appears that liver fibrosis causes densification of collagen structures while the network topology is preserved. This situation can be modeled by an increasing order of recursions of self-similar structures which furthermore would represent the opposite case of thinning of the neuronal network due to aging or MS. Another very relevant application of structure elucidation by MRE was demonstrated by Sinkus *et al* (2007), showing a clear increase of α in breast tumors which was assigned to the enhanced vascularization of cancer tissue.

Other elastography studies of skeletal muscle based on continuous harmonic shear waves used higher vibration frequencies than those applied in our experiments (Dresner *et al* 2001, Sack *et al* 2002, Uffmann *et al* 2004, Papazoglou *et al* 2005, Papazoglou *et al* 2006, Bensamoun *et al* 2006, 2007, Hoyt *et al* 2008). Given the strong dispersion of G^* in table 1, no direct one-to-one comparison of elastic modulus values of our study with those obtained at higher drive frequencies is feasible. However, under assumption of a powerlaw for the storage modulus, an extrapolation of the mean G' values in table 1 yields at 120 Hz driving frequency, as used by Bensamoun *et al* (2006), a storage modulus of 3.9 kPa in the relaxed state and 7.5 kPa in contraction, which is in good agreement to 3.9 ± 1.2 kPa and 6.4 ± 1.8 kPa, respectively, measured in Bensamoun *et al* (2006). Hoyt *et al* (2008) observed the propagation of the ST mode along the fiber direction of the M. rectus femoris by sonoelastography and determined an elastic modulus by fitting the acquired dispersion relations of the phase velocity to the viscoelastic Voigt model. The reported values of approximately 5.5 kPa (relaxed muscle) and 10.5 kPa (contracted muscle) correspond to a mean driving frequency of 140 Hz and agree well with our extrapolated G' of 4.6 kPa and 9.5 kPa for both respective states of muscle activity. Slight variances are expected due to technical differences between multifrequency MRE and sonoelastography, which examine different wave modes in different planes and regions of thigh muscle.

In summary, a multifrequency MRE protocol of *in vivo* muscle was proposed and successfully tested on human thigh muscle. The experiments revealed that the complex modulus of muscle in the intermediate dynamic range displays a higher slope upon frequency when the muscle is activated. Analyzing the modulus function by a powerlaw model suggests that in both states of relaxed and contracted muscle the dynamic shear modulus displays scaling with a higher degree of freedom in the mechanical network when the muscle is contracted.

Acknowledgment

The authors are thankful to Professor Christian Friedrich from the University of Freiburg, Germany, for helpful discussions. Financial support of the German Research Foundation (grant SA 901/3) is gratefully acknowledged.

Appendix

In the following, we will adopt the theory of the dynamics of polymers in solution for illustrating fundamental features of the complex modulus in mesh-like viscoelastic networks. Let $\mathbf{r}_l(t) = [x_l(t), y_l(t), z_l(t)]^T$ denote the displacement (away from the equilibrium) of the l th bead of a network of N identical beads with tiny mass connected by linear springs with constant K . Assume that this network of coupled harmonic oscillators is surrounded by a viscous fluid at temperature T . The motion of the l th bead is then described by the Langevin equation,

$$\xi \dot{\mathbf{r}}_l + K A_{lm} \mathbf{r}_m = \mathbf{f}_l^{(\text{sto})}(t) + \mathbf{f}_l^{(\text{ext})}(t), \quad (\text{A.1})$$

where ξ is the constant of friction of each bead with the substrate. (A_{lm}) denotes the connectivity matrix (which indicates the connection between beads), and summation from 1 to N is implied by repeated indices (Doi and Edwards 1986). The inhomogeneous terms are a stochastic force $f^{(\text{sto})}$ arising due to random collisions of fluid particles with the beads and the external force $f^{(\text{ext})}$, which is due to the external harmonic vibration. The thermal noise $f^{(\text{sto})}$ is assumed to be Gaussian with zero mean and $\langle f_{\alpha l}^{(\text{sto})}(t) f_{\beta m}^{(\text{sto})}(t') \rangle = 2k_B T \xi \delta_{\alpha\beta} \delta_{lm} \delta(t - t')$, with the angles representing configurational averages and Greek indices denoting Cartesian components. k_B is Boltzmann's constant. Under the assumption of external harmonic shearing $\mathbf{f}_l^{(\text{ext})} = [\xi g_0 e^{i\omega t} y_l(t), 0, 0]^T$, where g_0 is a velocity gradient, the z component of \mathbf{r} decouples and the equations of motion for the remaining components read

$$\begin{aligned} \xi [\dot{x}_l(t) - g_0 e^{i\omega t} y_l(t)] + K A_{lm} x_m(t) &= f_{xl}^{(\text{sto})} \\ \xi \dot{y}_l(t) + K A_{lm} y_m(t) &= f_{yl}^{(\text{sto})}. \end{aligned} \quad (\text{A.2})$$

The complex modulus $G^*(\omega)$ of the network can be deduced from the additional work $W(\omega)$ per unit volume done by the external shearing force on the network due to the presence of the surrounding substrate (Doi and Edwards 1986, Gurtovenko and Blumen 2005):

$$G^*(\omega) = \frac{i\omega}{g_0^2} W(\omega) = -\frac{i\omega}{V g_0^2} \langle \mathbf{F}_l \cdot v_l^* \rangle, \quad (\text{A.3})$$

where \mathbf{F}_l is the force by which the viscous substrate acts on the l th bead and v_l^* is the complex conjugate of the fluid velocity at that position. If one neglects for a moment the stochastic force in the first equation of (A.2), one finds the force on the l th bead and hence for the additional work

$$W(\omega) = \frac{1}{V} g_0 \exp(-i\omega t) K A_{lm} \langle x_m(t) y_l(t) \rangle. \quad (\text{A.4})$$

Equations (A.2) are coupled due to the connectivity matrix and the external force. Transformation to normal coordinates diagonalizes (A_{lm}) . Denoting $\mathbf{q}_k = [q_{1k}(t), q_{2k}(t), q_{3k}(t)]^T$, the additional work reads

$$W(\omega) = \frac{1}{V} g_0 \exp(-i\omega t) \lambda_k \langle q_{1k}(t) q_{2k}(t) \rangle, \quad (\text{A.5})$$

with λ_k as eigenvalues of (A_{lm}) and unit volume V . An equation for the correlation function $\langle q_{1k}(t) q_{2k}(t) \rangle$ can be derived from equation (A.2). After transformation to normal coordinates,

the resulting equations are multiplied by q_{2k} . Using the property $q_{\alpha k} = q_{\alpha k}(0) \exp(-t/\tau_k)$, where $\tau_k = \xi/K/\lambda_k$ and the property $\langle q_{\alpha k}(t) f_{\beta k}^{(\text{sto})} \rangle = k_B T \delta_{\alpha\beta}$, one finds in equilibrium

$$\langle q_{1k}(t)q_{2k}(t) \rangle = k_B T g_0 \exp(i\omega t) \frac{\tau_k/2}{K\lambda_k(1+i\omega\tau_k/2)}. \quad (\text{A.6})$$

Consequently, the reduced complex modulus is given by

$$\frac{G^*(\omega)}{C} = \frac{1}{N} \sum_{k=2}^N \frac{i\omega\tau_k/2}{1+i\omega\tau_k/2} \quad \text{with} \quad C = \frac{Nk_B T}{V}. \quad (\text{A.7})$$

Equation (A.7) represents the superposition of N mechanical modes with relaxation times half those of the normal modes (τ_k). Each normal mode is produced by a single spring–dashpot unit where the spring and the dashpot are aligned in series as represented by the Maxwell model. Therefore, the complex modulus of the Maxwell element, $G^*(\omega) = \mu i\omega\tau/(1+i\omega\tau)$, resembles equation (A.7) for one mode with $\tau = \eta/\mu = \tau_k/2$.

References

- Asbach P, Klatt D, Hamhaber U, Braun J, Somasundaram R, Hamm B and Sack I 2008 Assessment of liver viscoelasticity using multifrequency MR elastography *Magn. Reson. Med.* **60** 373–9
- Asbach P, Klatt D, Schlosser B, Biermer M, Muche M, Rieger A, Loddenkemper C, Somasundaram R, Berg T, Hamm B, Braun J and Sack I 2010 Viscoelasticity-based staging of hepatic fibrosis with multifrequency MR elastography *Radiology* **257** 80–6
- Basford J R, Jenkyn T R, An K N, Ehman R L, Heers G and Kaufman K R 2002 Evaluation of healthy and diseased muscle with magnetic resonance elastography *Arch. Phys. Med. Rehabil.* **83** 1530–6
- Bensamoun S F, Ringleb S I, Chen Q, Ehman R L, An K N and Brennan M 2007 Thigh muscle stiffness assessed with magnetic resonance elastography in hyperthyroid patients before and after medical treatment *J. Magn. Reson. Imaging* **26** 708–13
- Bensamoun S F, Ringleb S I, Littrell L, Chen Q, Brennan M, Ehman R L and An K N 2006 Determination of thigh muscle stiffness using magnetic resonance elastography *J. Magn. Reson. Imaging* **23** 242–7
- Blange T, Van Der Heide U A, Treijtel B W and de Beer E L 1997 The effect of actin filament compliance on the interpretation of the elastic properties of skeletal muscle fibres *J. Muscle Res. Cell Motil.* **18** 125–31
- Blumen A and Jurjiu A 2002 Multifractal spectra and the relaxation of model polymer networks *J. Chem. Phys.* **116** 2636–41
- Brauck K, Galban C J, Maderwald S, Herrmann B L and Ladd M E 2007 Changes in calf muscle elasticity in hypogonadal males before and after testosterone substitution as monitored by magnetic resonance elastography *Eur. J. Endocrinol.* **156** 673–8
- Carcione J 2007 *Wave Fields in Real Media: Wave Propagation in Anisotropic, Anelastic, Porous and Electromagnetic Media* (Amsterdam: Elsevier)
- Deffieux T, Montaldo G, Tanter M and Fink M 2009 Shear wave spectroscopy for *in vivo* quantification of human soft tissues visco-elasticity *IEEE Trans. Med. Imaging* **28** 313–22
- Doi M and Edwards S F 1986 *The Theory of Polymer Dynamics* vol 73 (New York: Oxford University Press)
- Domire Z J, McCullough M B, Chen Q S and An K N 2009 Wave attenuation as a measure of muscle quality as measured by magnetic resonance elastography: initial results *J. Biomech.* **42** 537–40
- Dresner M A, Rose G H, Rossman P J, Muthupillai R, Manduca A and Ehman R L 2001 Magnetic resonance elastography of skeletal muscle *J. Magn. Reson. Imaging* **13** 269–76
- Friedrich C 1991 Relaxation functions of rheological constitutive equations with fractional derivatives: thermodynamical constraints *Rheological Modelling: Thermodynamical and Statistical Approaches (Lecture Notes in Physics* vol 381) pp 321–30
- Gennisson J L, Catheline S, Chaffai S and Fink M 2003 Transient elastography in anisotropic medium: application to the measurement of slow and fast shear wave speeds in muscles *J. Acoust. Soc. Am.* **114** 536–41
- Gennisson J L, Cornu C, Catheline S, Fink M and Portero P 2005 Human muscle hardness assessment during incremental isometric contraction using transient elastography *J. Biomech.* **38** 1543–50
- Gennisson J L, Deffieux T, Mace E, Montaldo G, Fink M and Tanter M 2010 Viscoelastic and anisotropic mechanical properties of *in vivo* muscle tissue assessed by supersonic shear imaging *Ultrasound Med. Biol.* **36** 789–801
- Gurtovenko A A and Blumen A 2005 *Polymer Analysis, Polymer Theory* (Berlin: Springer) pp 171–282

- Heers G, Jenkyn T, Dresner M A, Klein M O, Basford J R, Kaufman K R, Ehman R L and An K N 2003 Measurement of muscle activity with magnetic resonance elastography *Clin. Biomech. (Bristol, Avon)* **18** 537–42
- Hoyt K, Kneezel T, Castaneda B and Parker K J 2008 Quantitative sonoelastography for the *in vivo* assessment of skeletal muscle viscoelasticity *Phys. Med. Biol.* **53** 4063–80
- Jenkyn T R, Ehman R L and An K N 2003 Noninvasive muscle tension measurement using the novel technique of magnetic resonance elastography (MRE) *J. Biomech.* **36** 1917–21
- Jurjiiu A, Friedrich C and Blumen A 2002 Strange kinetics of polymeric networks modelled by finite fractals *Chem. Phys.* **284** 221–31
- Klatt D, Asbach P, Rump J, Papazoglou S, Somasundaram R, Modrow J, Braun J and Sack I 2006 *In vivo* determination of hepatic stiffness using steady-state free precession magnetic resonance elastography *Invest. Radiol.* **41** 841–8
- Klatt D, Asbach P, Somasundaram R, Hamm B, Braun J and Sack I 2008 Assessment of the solid-liquid behavior of the liver for the diagnosis of diffuse disease using magnetic resonance elastography *Rofo-Fortschr. Geb. Rontgenstr. Bildgeb. Verfahr.* **180** 1104–9
- Klatt D, Friedrich C, Korth Y, Vogt R, Braun J and Sack I 2010 Viscoelastic properties of liver measured by oscillatory rheometry and multifrequency magnetic resonance elastography *Biorheology* **47** 133–41
- Klatt D, Hamhaber U, Asbach P, Braun J and Sack I 2007 Noninvasive assessment of the rheological behavior of human internal organs using multifrequency MR elastography: a study of brain and liver viscoelasticity *Phys. Med. Biol.* **52** 7281–94
- Musgrave M J P 1970 *Crystal Acoustics* (San Francisco, CA: Holden-Day)
- Muthupillai R, Lomas D J, Rossman P J, Greenleaf J F, Manduca A and Ehman R L 1995 Magnetic resonance elastography by direct visualization of propagating acoustic strain waves *Science* **269** 1854–7
- Papazoglou S, Braun J, Hamhaber U and Sack I 2005 Two-dimensional waveform analysis in MR elastography of skeletal muscles *Phys. Med. Biol.* **50** 1313–25
- Papazoglou S, Rump J, Braun J and Sack I 2006 Shear-wave group-velocity inversion in MR elastography of human skeletal muscle *Magn. Reson. Med.* **56** 489–97
- Plewes D B, Betty I, Urchuk S N and Soutar I 1995 Visualizing tissue compliance with MR imaging *J. Magn. Reson. Imaging* **5** 733–8
- Ringleb S I, Bensamoun S F, Chen Q, Manduca A, An K N and Ehman R L 2007 Applications of magnetic resonance elastography to healthy and pathologic skeletal muscle *J. Magn. Reson. Imaging* **25** 301–9
- Romano A J, Abraham P B, Rossman P J, Bucaro J A and Ehman R L 2005 Determination and analysis of guided wave propagation using magnetic resonance elastography *Magn. Reson. Med.* **54** 893–900
- Rouse P E 1953 A theory of the linear viscoelastic properties of dilute solutions of coiling polymers *J. Chem. Phys.* **21** 1272–80
- Sack I, Beierbach B, Wuerfel J, Klatt D, Hamhaber U, Papazoglou S, Martus P and Braun J 2009 The impact of aging and gender on brain viscoelasticity *Neuroimage* **46** 652–7
- Sack I, Bernarding J and Braun J 2002 Analysis of wave patterns in MR elastography of skeletal muscle using coupled harmonic oscillator simulations *Magn. Reson. Imaging* **20** 95–104
- Schiessel H and Blumen A 1995 Mesoscopic pictures of the sol-gel transition—ladder models and fractal networks *Macromolecules* **28** 4013–9
- Schiessel H, Metzler R, Blumen A and Nonnenmacher T F 1995 Generalized viscoelastic models: their fractional equations with solutions *J. Phys. A: Math. Gen.* **28** 6567–84
- Schmalbruch H 1985 *Skeletal Muscle* (Berlin: Springer)
- Sinkus R, Tanter M, Catheline S, Lorenzen J, Kuhl C, Sondermann E and Fink M 2005 Imaging anisotropic and viscous properties of breast tissue by magnetic resonance elastography *Magn. Reson. Med.* **53** 372–87
- Sinkus R, Siegmann K, Xydeas T, Tanter M, Claussen C and Fink M 2007 MR elastography of breast lesions: understanding the solid/liquid duality can improve the specificity of contrast-enhanced MR mammography *Magn. Reson. Med.* **58** 1135–44
- Uffmann K, Maderwald S, Ajjaj W, Galban C G, Mateiescu S, Quick H H and Ladd M E 2004 *In vivo* elasticity measurements of extremity skeletal muscle with MR elastography *NMR Biomed.* **17** 181–90
- Wuerfel J, Paul F, Beierbach B, Hamhaber U, Klatt D, Papazoglou S, Zipp F, Martus P, Braun J and Sack I 2010 MR-elastography reveals degradation of tissue integrity in multiple sclerosis *Neuroimage* **49** 2520–5